Radiocarbon Measurements. Uranium–Thorium Decay Series in the Oceans Overview.

Further Reading

Guary JC, Guegueniat P and Pentreath RJ (eds) (1988) *Radionuclides: A Tool for Oceanography*. London, New York: Elsevier Applied Science.

Hunt GJ, Kershaw PJ and Swift DJ (eds) (1998) Radionuclides in the oceans (RADOC 96–97). Distribution, Models and Impacts. *Radiation Protection Dosimetry* 75 (1–4) 1998.

IAEA (1995) *Environmental impact of radioactive releases;* Proceedings of an International Symposium on Environmental Impact of Radioactive Releases. International Atomic Energy Agency, Vienna, 1995.

IAEA (1999) *Inventory of Radioactive Waste Disposals at Sea*. IAEA-TECDOC-1105. International Atomic Energy Agency, Vienna, August 1999, pp. 24 A.1–A.22.

RADIOCARBON

R. M. Key, Princeton University, Princeton, NJ, USA

doi:10.1006/rwos.2001.0162

Introduction

In 1934 F.N.D. Kurie at Yale University obtained the first evidence for existence of radiocarbon (carbon-14, ^{14}C). Over the next 20 years most of the details for measuring ^{14}C and for its application to dating were worked out by W.F. Libby and co-workers. Libby received the 1960 Nobel Prize in chemistry for this research.

The primary application of ^{14}C is to date objects or to determine various environmental process rates. The ^{14}C method is based on the assumption of a constant atmospheric formation rate. Once produced, atmospheric ^{14}C reacts to form $^{14}CO_2$, which participates in the global carbon cycle processes of photosynthesis and respiration as well as the physical processes of dissolution, particulate deposition, evaporation, precipitation, transport, etc. Atmospheric radiocarbon is transferred to the ocean primarily by air–sea gas exchange of $^{14}CO_2$. Once in the ocean, $^{14}CO_2$ is subject to the same physical, chemical, and biological processes that affect CO_2. While alive, biota establish an equilibrium concentration of radiocarbon with their surroundings; that is, ^{14}C lost by decay is replaced by uptake from the environment. Once the tissue dies or is removed from an environment that contains ^{14}C, the decay is no longer compensated. The loss of ^{14}C by decay can then be used to determine the time of death or removal from the original ^{14}C source. After death or removal of the organism, it is generally assumed that no exchange occurs between the tissue and its surroundings; that is, the system is assumed to be closed. As a result of the ^{14}C decay rate, the various reservoir sizes involved in the carbon cycle, and exchange rates between the reservoirs, the ocean contains approximately 50 times as much natural radiocarbon as does the atmosphere.

Carbon-14 is one of three naturally occurring carbon isotopes; ^{14}C is radioactive, has a half-life of 5730 years and decays by emitting a β-particle with an energy of about 156 keV. On the surface of the earth, the abundance of natural ^{14}C relative to the two stable naturally occurring carbon isotopes is $^{12}C : {}^{13}C : {}^{14}C = 98.9\% : 1.1\% : 1.2 \times 10^{-10}\,\%$. Natural radiocarbon is produced in the atmosphere, primarily by the collision of cosmic ray produced neutrons with nitrogen according to the reaction [I].

$$ {}^{1}_{0}\mathrm{n} + {}^{14}_{7}\mathrm{N} \Rightarrow {}^{14}_{6}\mathrm{C} + {}^{1}_{1}\mathrm{H} \qquad [\mathrm{I}] $$

where n is a neutron and H is the proton emitted by the product nucleus. Similarly, the decay of ^{14}C takes place by emission of a β-particle and leads to stable nitrogen according to reaction [II],

$$ {}^{14}_{6}\mathrm{C} \Rightarrow {}^{14}_{7}\mathrm{N} + \beta^{-} + \bar{\nu} + Q \qquad [\mathrm{II}] $$

where $\bar{\nu}$ is an antineutrino and Q is the decay energy.

The atmospheric production rate varies somewhat and is influenced by changes in the solar wind and in the earth's geomagnetic field intensity. A mean of $1.57\,\mathrm{atom\,cm^{-2}\,s^{-1}}$ is estimated based on the long-term record preserved in tree rings and a carbon reservoir model. This long-term production rate yields a global natural ^{14}C inventory of approximately 50 t ($1\,\mathrm{t} = 10^{6}\,\mathrm{g}$). Production estimates based on the more recent record of neutron flux measurements tend to be higher, with values approaching $2\,\mathrm{atom\,cm^{-2}\,s^{-1}}$. **Figure 1** shows the atmospheric history of ^{14}C from AD 1511 to AD 1954 measured by Minze Stuiver (University of Washington) using tree growth rings. The strong decrease that occurs

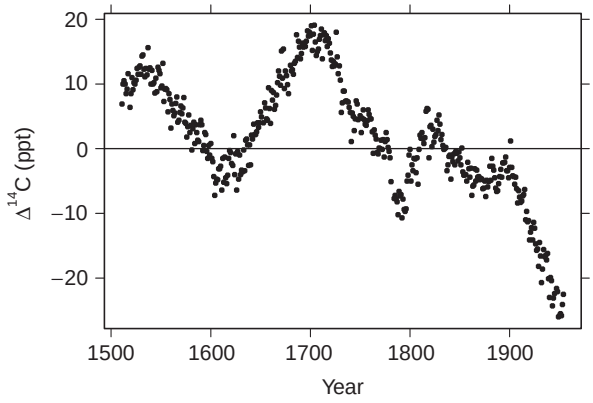

Figure 1 Atmospheric history of $\Delta^{14}C$ measured by M. Stuiver in tree rings covering AD 1511 to AD 1954. Most of the decrease over the last hundred years is due to the addition of anthropogenic CO_2 to the atmosphere during the industrial revolution by the burning of fossil fuels.

after about AD 1880 is due to dilution by anthropogenic addition of CO_2 during the industrial revolution by the burning of fossil fuels (coal, gas, oil). This dilution has come to be known as the Suess effect (after Hans E. Suess).

Prior to 16 July 1945 all radiocarbon on the surface of the earth was produced naturally. On that date, US scientists carried out the first atmospheric atomic bomb test, known as the Trinity Test. Between 1945 and 1963, when the Partial Test Ban Treaty was signed and atmospheric nuclear testing was banned, approximately 500 atmospheric nuclear explosions were carried out by the United States (215), the former Soviet Union (219), the United Kingdom (21) and France (50). After the signing, a few additional atmospheric tests were carried out by China (23) and other countries not participating in the treaty. The net effect of the testing was to significantly increase ^{14}C levels in the atmosphere and subsequently in the ocean. Anthropogenic ^{14}C has also been added to the environment from some nuclear power plants, but this input is generally only detectable near the reactor.

It is unusual to think of any type of atmospheric contamination – especially by a radioactive species – as beneficial; however, bomb-produced radiocarbon (and tritium) has proven to be extremely valuable to oceanographers. The majority of the atmospheric testing, in terms of number of tests and ^{14}C production, occurred over a short time interval, between 1958 and 1963, relative to many ocean circulation processes. This time history, coupled with the level of contamination and the fact that ^{14}C becomes intimately involved in the oceanic carbon cycle, allows bomb-produced radiocarbon to be valuable as a tracer for several ocean processes including biological activity, air–sea gas exchange, thermocline ventilation, upper ocean circulation, and upwelling.

Oceanographic radiocarbon results are generally reported as $\Delta^{14}C$, the activity ratio relative to a standard (NBS oxalic acid, 13.56 dpm per g of carbon) with a correction applied for dilution of the radiocarbon by anthropogenic CO_2 with age corrections of the standard material to AD 1950. $\Delta^{14}C$ is defined by eqn [1].

$$\Delta^{14}C = \delta^{14}C - 2(\delta^{13}C + 25)\left(1 + \frac{\delta^{14}C}{1000}\right) \quad [1]$$

$\delta^{14}C$ is given by eqn [2] and the definition of $\delta^{13}C$ is analogous to that for $\delta^{14}C$.

$$\delta^{14}C = \left[\frac{^{14}C/C|_{smp} - {}^{14}C/C|_{std}}{^{14}C/C|_{std}}\right] \times 1000 \quad [2]$$

The first part of the second term in the right side of eqn [1] $2(\delta^{13}C + 25)$, corrects for fractionation effects. The factor of 2 accounts for the fact that ^{14}C fractionation is expected to be twice as much as for ^{13}C and the additive constant 25 is a normalization factor conventionally applied to all samples and based on the mean value of terrestrial wood. The details of ^{14}C calculations can be significantly more involved than expressed in the above equations; however, there is a general consensus that the calculations and reporting of results be done as described by Minze Stuiver and Henry Polach in a paper specifically written to eliminate differences that existed previously. $\Delta^{14}C$ has units of parts per thousand (ppt). That is, 1 ppt means that $^{14}C/^{12}C$ for the sample is greater than $^{14}C/^{12}C$ for the standard by 0.001. In these units the radioactive decay rate of ^{14}C is approximately 1 ppt per 8.1 years.

The number of surface ocean measurements made before any bomb-derived contamination are insufficient to provide the global distribution before input from explosions. It is now possible to measure $\Delta^{14}C$ values in the annual growth rings of corals. By establishment of the exact year associated with each ring, reconstruction of the surface ocean $\Delta^{14}C$ history is possible. Applying the same procedure to long-lived mollusk shells extends the method to higher latitudes than is possible with corals. Whether corals or shells are used, it must be demonstrated that the coral or shell incorporates ^{14}C in the same ratio as the water in which it grew or at least that the fractionation is known. This method works only over the depth range at which the animal lived.

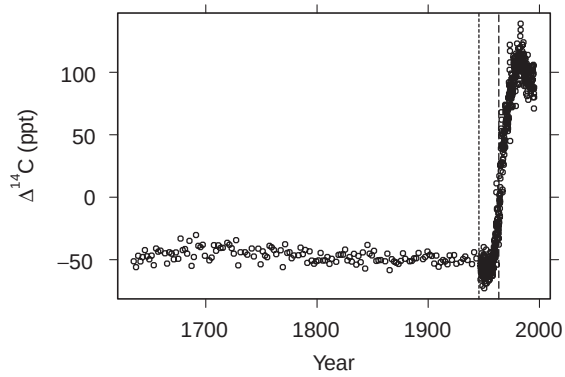

Figure 2 Long-term history of $\Delta^{14}C$ in the surface Pacific Ocean measured by E. Druffel in two coral reefs. The vertical lines surround the period of atmospheric nuclear weapons testing. The oceanic response to bomb contamination is delayed relative to the atmosphere because of the relatively long equilibration time between the ocean and atmosphere for $^{14}CO_2$.

Figure 2 shows the $\Delta^{14}C$ record from two Pacific coral reefs measured by Ellen Druffel. Vertical lines indicate the period of atmospheric nuclear tests (1945–1963). The relatively small variability over the first ~300 years of the record includes variations due to weather events, climate change, ocean circulation, atmospheric production, etc. The last 50 years of the sequence records the invasion of bomb-produced $\Delta^{14}C$. Worth noting is the fact that the coral record of the bomb signal is lagged. That is, the coral values did not start to increase immediately testing began nor did they cease to increase when atmospheric testing ended. The lag is due to the time for the northern and southern hemisphere atmospheres to mix (~1 year) and to the relatively long time required for the surface ocean to equilibrate with the atmosphere with respect to $\Delta^{14}C$ (~10 years). Because of the slow equilibration, the surface ocean is frequently not at equilibrium with the atmosphere. This disequilibrium is one of the reasons why pre-bomb surface ocean results, when expressed as ages rather than ppt units, are generally 'old' rather than 'zero' as might be expected.

Figure 3A shows measured atmospheric $\Delta^{14}C$ levels from 1955 to the present in New Zealand (data from T.A. Rafter, M.A. Manning, and co-workers) and Germany (data from K.O. Munnich and co-workers) as well as older estimates based on tree ring measurements (data from M. Stuiver). The beginning of the significant increase in the mid-1950s marks the atmospheric testing of hydrogen bombs. Atmospheric levels increased rapidly from that point until the mid-1960s. Soon after the ban on atmospheric testing, levels began a decrease that continues up to the present. The rate of decrease in the atmosphere is about $0.055\,y^{-1}$. Also clearly evident in the figure is that the German measurements were significantly higher than those from New Zealand between approximately 1962 and 1970. The difference reflects the facts that most of the atmospheric tests were carried out in the Northern Hemisphere and that approximately 1 year is required for atmospheric mixing across the Equator. During that interval some of the atmospheric $^{14}CO_2$ is removed. Once atmospheric testing ceased, the two hemispheres equilibrated to the same radiocarbon level.

Figure 3B shows detailed Pacific Ocean $\Delta^{14}C$ coral ring data (J.R. Toggwelier and E. Druffel). This surface ocean record shows an increase during the 1960s; however, the peak occurs somewhat later than in the atmosphere and is significantly less

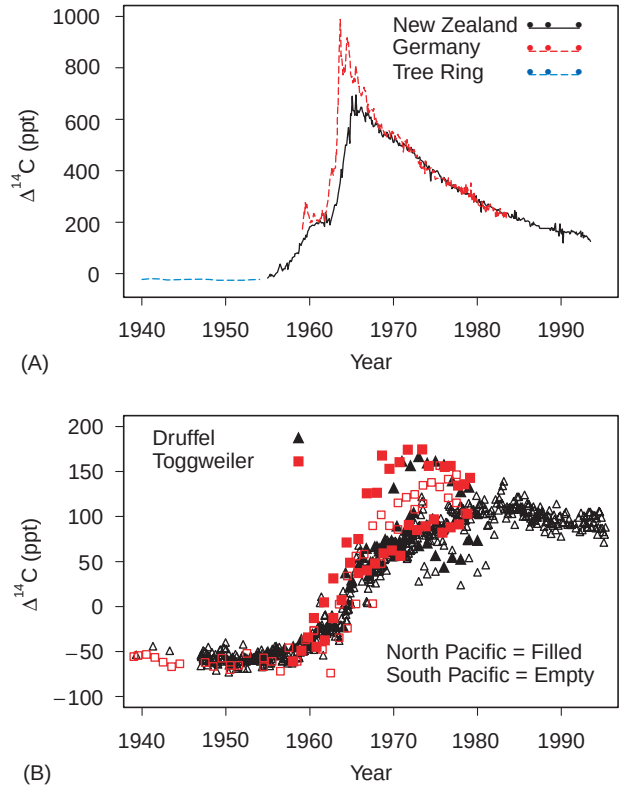

Figure 3 (A) Detailed atmospheric $\Delta^{14}C$ history as recorded in tree rings for times prior to 1955 and in atmospheric gas samples from both New Zealand and Germany subsequently. The large increase in the late 1950s and 1960s was due to the atmospheric testing of nuclear weapons (primarily fusion devices). The hemispheric difference during the 1960s is because most atmospheric bomb tests were carried out north of the Equator and there is a resistance to atmospheric mixing across the equator. Atmospheric levels began to decline shortly after the ban on atmospheric bomb testing. (B) $\Delta^{14}C$ in the surface Pacific Ocean as recorded in the annual growth rings of corals. The same general trend seen in the atmosphere is present. The bomb contamination peak is broadened and time-lagged relative to the atmosphere due to both mixing and to the time required for transfer from the atmosphere to the ocean.

pronounced. Careful investigation of coral data also demonstrates the north–south difference evidenced in the atmospheric record.

Sampling and Measurement Techniques

The radiocarbon measurement technique has existed for only 50 years. The first ^{14}C measurement was made in W.F. Libby's Chicago laboratory in 1949 and the first list of ages was published in 1951. A necessary prerequisite to the age determination was accurate measurement of the radiocarbon half-life. This was done in 1949 in Antonia Engelkeimer's laboratory at the Argonne National Laboratory. Between 1952 and 1955 several additional radiocarbon dating laboratories opened. By the early 1960s several important advances had occurred including the following.

- Significantly improved counting efficiency and lower counting backgrounds, resulting in much greater measurement precision and longer timescale over which the technique was applicable.
- Development of the extraction and concentration technique for sea water samples.
- More precise determination of the half-life by three different laboratories.
- Recognition by Hans Suess, while at the USGS and Scripps Institution of Oceanography, that radiocarbon in modern samples (since the beginning of the industrial revolution) was being diluted by anthropogenic CO_2 addition to the atmosphere and biosphere.
- Recognition that atmospheric and oceanic $\Delta^{14}C$ levels were increasing as a result of atmospheric testing of nuclear weapons.

During the 1970s and 1980s incremental changes in technique and equipment further increased the precision and lowered the counting background. With respect to the ocean, this was a period of sample collection, analysis, and interpretation. The next significant change occurred during the 1990s with application of the accelerator mass spectrometry (AMS) technique to oceanic samples. This technique counts ^{14}C atoms rather than detecting the energy released when a ^{14}C atom decays. The AMS technique allowed reduction of the sample size required for oceanic $\Delta^{14}C$ determination from approximately 250 liters of water to 250 milliliters! By 1995 the AMS technique was yielding results that were as good as the best prior techniques using large samples and decay counting. This size reduction and concurrent automation procedures had a profound effect on sea water $\Delta^{14}C$ determination. Many of the AMS techniques were developed and most of the oceanographic AMS $\Delta^{14}C$ measurements have been made at the National Ocean Sciences AMS facility in Woods Hole, Massachusetts, by Ann McNichol, Robert Schneider, and Karl von Reden under the initial direction of Glenn Jones and more recently John Hayes.

The natural concentration of ^{14}C in sea water is extremely low ($\sim 1 \times 10^9$ atoms kg^{-1}). Prior to AMS, the only available technique to measure this low concentration was radioactive counting using either gas proportional or liquid scintillation detectors. Large sample were needed to obtain high precision and to keep counting times reasonable. Between about 1960 and 1995 most subsurface open-ocean radiocarbon water samples were collected using a Gerard–Ewing sampler commonly known as a Gerard barrel. The final design of the Gerard barrel consisted of a stainless steel cylinder with a volume of approximately 270 liters. An external scoop and an internal divider running the length of the cylinder resulted in efficient flushing while the barrel was lowered through the water on wire rope. When the barrel was returned to the ship deck, the water was transferred to a gas-tight container and acidified to convert carbonate species to CO_2. The CO_2 was swept from the water with a stream of inert gas and absorbed in a solution of sodium hydroxide. The solution was returned to shore where the CO_2 was extracted, purified, and counted. When carefully executed, the procedure produced results which were accurate to 2–4 ppt based on counting errors alone. Because of the expense, time, and difficulty, samples for replicate analyses were almost never collected.

With the AMS technique only 0.25 liter of sea water is required. Generally a 0.5 liter water sample is collected at sea and poisoned with $HgCl_2$ to halt all biological activity. The water is returned to the laboratory and acidified, and the CO_2 is extracted and purified. An aliquot of the CO_2 is analyzed to determine $\delta^{13}C$ and the remainder is converted to carbide and counted by AMS. Counting error for the AMS technique can be < 2 ppt, however, replicate analysis shows the total sample error to be approximately 4.5 ppt.

Sampling History

Soon after the radiocarbon dating method was developed, it was applied to oceanic and atmospheric samples. During the 1950s and 1960s most of the oceanographic samples were limited to the shallow

waters owing to the difficulty of deep water sampling combined with the limited analytical precision. The majority of the early samples were collected in the Atlantic Ocean and the South-west Pacific Ocean. Early sample coverage was insufficient to give a good description of the global surface ocean radiocarbon content prior to the onset of atmospheric testing of thermonuclear weapons; however, repeated sampling at the same location was sufficient to record the surface water increase due to bomb-produced fallout. A very good history of radiocarbon activity, including the increase due to bomb tests and subsequent decrease, exists primarily as a result of the work of R. Nydal and co-workers (Trondheim) and K. Munnich and co-workers (Heidelberg).

The primary application of early radiocarbon results was to estimate the flux of CO_2 between the atmosphere and ocean and the average residence time in the ocean. Sufficient subsurface ocean measurements were made, primarily by W. Broecker (Lamont–Doherty Earth Observatory LDEO) and H. Craig (Scripps Institution of Oceanography SIO), to recognize that radiocarbon had the potential to be an important tracer of deep ocean circulation and mixing rates.

During the 1970s the Geochemical Ocean Sections (GEOSECS) program provided the first full water column global survey of the oceanic radiocarbon distribution. The GEOSECS cruise tracks were approximately meridional through the center of the major ocean basins. Radiocarbon was sampled with a station spacing of approximately 500 km and an average of 20 samples per station. All of the GEOSECS $\Delta^{14}C$ measurements were made by G. Östlund (University of Miami) and M. Stuiver (University of Washington) using traditional β counting of large-volume water samples with a counting accuracy of ~ 4 ppt. GEOSECS results revolutionized what was known about the oceanic $\Delta^{14}C$ distribution and the applications for which radiocarbon is used.

During the early 1980s the Atlantic Ocean was again surveyed for radiocarbon as part of the Transient Tracers in the Ocean (TTO) North Atlantic Study (NAS) and Tropical Atlantic Study (TAS) programs and the South Atlantic Ventilation Experiment (SAVE). Sampling for these programs was designed to enable mapping of property distributions on constant pressure or density surfaces with reasonable gridding uncertainty. The radiocarbon portion of these programs was directed by W. Broecker. Östlund made the $\Delta^{14}C$ measurements with $\delta^{13}C$ provided by Stuiver using the GEOSECS procedures. Comparison of TTO results to GEOSECS gave the first clear evidence of the penetration of the bomb-produced radiocarbon signal into the subsurface North Atlantic waters. The French carried out a smaller scale (INDIGO) ^{14}C program in the Indian Ocean during this time with Östlund and P. Quay (University of Washington) collaborating. These data also quantified upper ocean changes since GEOSECS and relied on the same techniques.

The most recent oceanic survey was carried out during the 1990s as part of the World Ocean Circulation Experiment (WOCE). This program was a multinational effort. The US ^{14}C sampling effort was heavily focused on the Pacific (1991–1993) and Indian oceans (1995–1996) since TTO and SAVE had provided reasonable Atlantic coverage. R. Key (Princeton University) directed the US radiocarbon effort with collaboration from P. Schlosser (LDEO) and Quay. In the deep Pacific where gradients were known to be small, most radiocarbon sampling was by the proven large-volume β technique. The Pacific thermocline, however, was sampled using the AMS technique. Shifting techniques allowed thermocline waters to be sampled at approximately 2–3 times the horizontal density used for large volume sampling. Östlund and Stuiver again measured the large-volume samples while the AMS samples were measured at the National Ocean Sciences AMS facility (NOSAMS) at Woods Hole Oceanographic Institution. By 1994 the analytical precision at NOSAMS had improved to the point that all US Indian Ocean WOCE ^{14}C sampling used this technique. WOCE sampling increased the total number of ^{14}C results for the Pacific and Indian Oceans by approximately an order of magnitude. Analysis of the Pacific Ocean samples was completed in 1998. US WOCE ^{14}C sampling in the Atlantic was restricted to two zonal sections in the north-west basin using the AMS technique. Analysis of the Atlantic and Indian Ocean samples is expected to be finished during 2000–2001.

$\Delta^{14}C$ Distribution and Implications for Large-scale Circulation

The distribution of radiocarbon in the ocean is controlled by the production rate in the atmosphere, the spatial variability and magnitude of $^{14}CO_2$ flux across the air–sea interface, oceanic circulation and mixing, and the carbon cycle in the ocean. **Figure 4** shows average vertical radiocarbon profiles for the Pacific, Atlantic, Southern, and Indian oceans with the dotted line being southern basin and solid line northern basin. All of the profiles have higher $\Delta^{14}C$

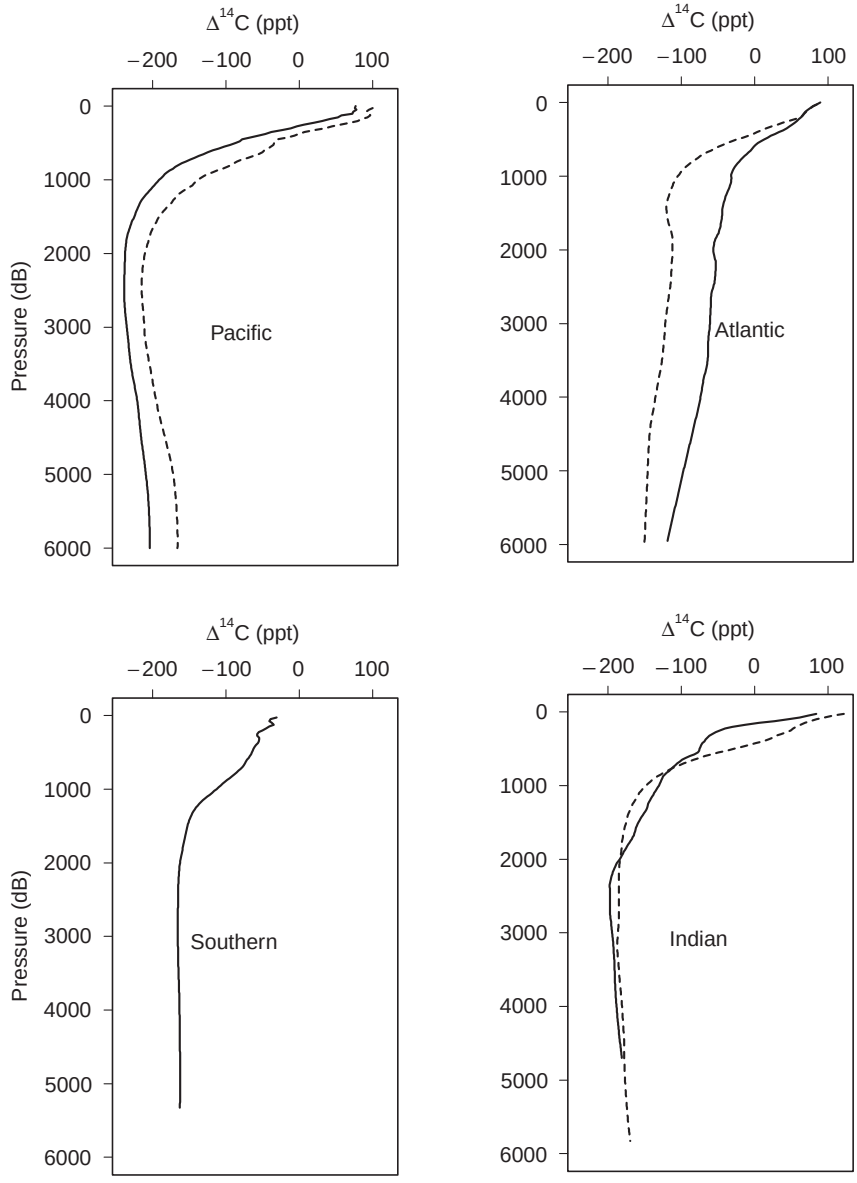

Figure 4 Average vertical $\Delta^{14}C$ profiles for the major ocean basins. Except for the Southern Ocean the dotted line is for the Southern Hemisphere and the solid line for the Northern Hemisphere. The Pacific and Southern Ocean profiles were compiled from WOCE data; the Atlantic profiles from TTO and SAVE data; and the Indian Ocean profiles from GEOSECS data. In approximately the upper 1000 m (=1000 dB) of each profile, the natural $\Delta^{14}C$ is contaminated with bomb-produced radiocarbon.

in shallow waters, reflecting proximity to the atmospheric source. The different collection times combined with the penetration of the bomb-produced signal into the upper thermocline negate the possibility of detailed comparison for the upper 600–800 dB (deeper for the North Atlantic). Detailed comparison is justified for deeper levels. The strongest signal in deep and bottom waters is that the North Atlantic is significantly younger (higher $\Delta^{14}C$) than the South Atlantic, while the opposite holds for the Pacific. Second, the average age of deep water increases ($\Delta^{14}C$ decreases) from Atlantic to Indian to Pacific. Third, the Southern Ocean $\Delta^{14}C$ is very uniform below approximately 1800 dB at a level (~ -160 ppt). This is similar to the near bottom water values for all three southern ocean basins. All three differences are directly attributable to the large-scale thermohaline circulation.

Figure 5 shows meridional sections for the Atlantic, Indian and Pacific oceans using subsets of the data from **Figure 4**. As with **Figure 4**, the $\Delta^{14}C$ values in the upper water column have been

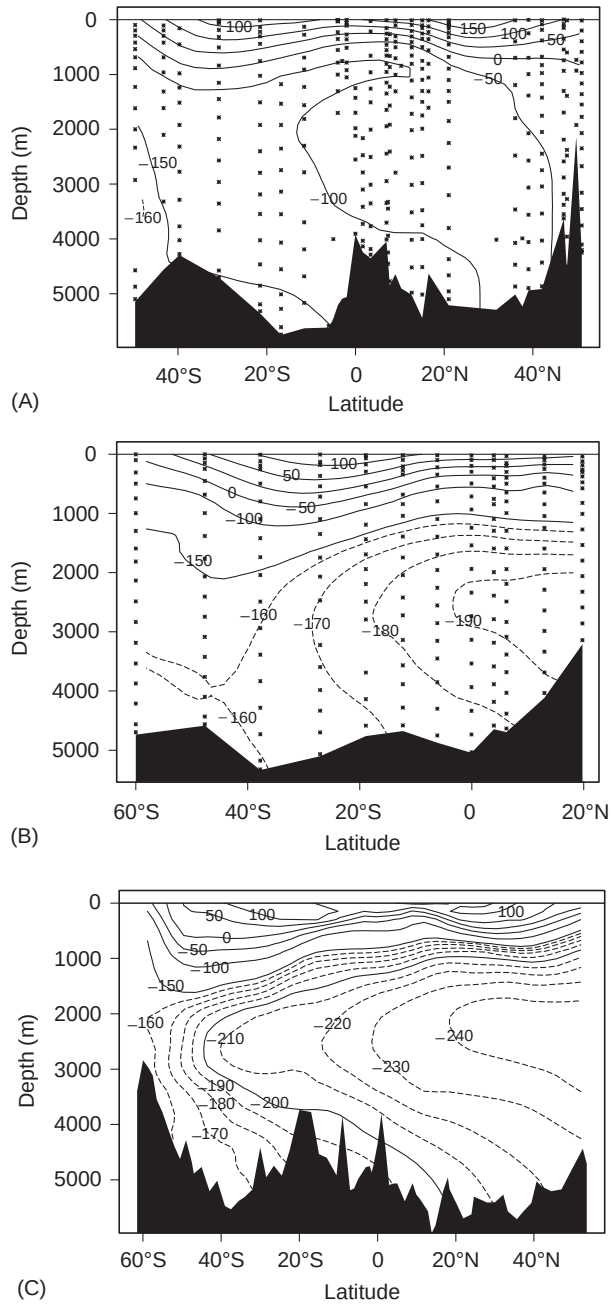

Figure 5 Typical meridional sections for each ocean compiled from a subset of the data used for **Figure 4**. The deep water contour patterns are primarily due to the large-scale thermohaline circulation. The highest deep water $\Delta^{14}C$ values are found in the North Atlantic and the lowest in the North Pacific. The natural $\Delta^{14}C$ in the upper ocean is contaminated by the influx of bomb-produced radiocarbon.

increased by invasion of the bomb signal. The pattern of these contours, however, is generally representative of the natural $\Delta^{14}C$ signal. The $\Delta^{14}C = -100‰$ contour can be taken as the approximate demarcation between the bomb-contaminated waters and those having only natural radiocarbon.

Comparison of the major features in each section shows that the meridional $\Delta^{14}C$ distributions in the Pacific and Indian Oceans are quite similar. The greatest difference between these two is that the Indian Ocean deep water (1500–3500 m) is significantly younger than Pacific deep waters. In both oceans:

- The near bottom water has higher $\Delta^{14}C$ than the overlying deep water.
- The deep and bottom waters have higher $\Delta^{14}C$ at the south than the north.
- The lowest $\Delta^{14}C$ values are found as a tongue extending southward from the north end of the section at a depth of $\sim$2500 m.
- Deep and bottom water at the south end of each section is relatively uniform with $\Delta^{14}C \sim -160$ ppt.
- The $\Delta^{14}C$ gradient with latitude from south to north is approximately the same for both deep waters and for bottom waters.
- The $\Delta^{14}C$ contours in the thermocline shoal both at the equator and high latitudes. (This feature is suppressed in the North Indian Ocean owing to the limited geographic extent and the influence of flows through the Indonesian Seas region and from the Arabian Sea.)

In the Atlantic Ocean the pattern in the shallow water down through the upper thermocline is similar to that in the other oceans. The $\Delta^{14}C$ distribution in the deep and bottom waters of the Atlantic is, however, radically different. The only similarities to the other oceans are (1) the $\Delta^{14}C$ value for deep and bottom water at the southern end of the section, (2) a southward-pointing tongue in deep water, and (3) the apparent northward flow indicated by the near-bottom tongue-shaped contour. Atlantic deep water has higher $\Delta^{14}C$ than the bottom water, and the deep and bottom waters at the north end of the section have higher rather that lower $\Delta^{14}C$ as found in the Indian and Pacific. Additionally, the far North Atlantic deep and bottom waters have relatively uniform values rather than a strong vertical gradient.

The reversal of the Atlantic deep and bottom water $\Delta^{14}C$ gradients with latitude relative to those in the Indian and Pacific is due to the fact that only the Atlantic has the conditions of temperature and salinity at the surface (in the Greenland–Norwegian Sea and Labrador Sea areas) that allow formation of a deep water mass (commonly referred to as North Atlantic Deep Water, NADW). Newly formed NADW flows down slope from the formation region until it reaches a level of neutral buoyancy. Flow is then southward, primarily as a deep western

boundary current constrained by the topography of the North American slope. In its southward journey, NADW encounters and overrides northward-flowing denser waters of circumpolar origin. This general circulation pattern can be very clearly demonstrated by comparing the invasion of the bomb-produced tritium and radiocarbon signals obtained during GEOSECS to those from the TTO programs. This large circulation pattern leads to the observed $\Delta^{14}C$ distribution in the deep Atlantic.

Since neither the Pacific nor the Indian Ocean has a northern hemisphere source of deep water, the large-scale circulation is simpler. The densest Pacific waters originate in the Southern Ocean and flow northward along the sea floor (Circumpolar Deep Water, CDW). In the Southern Ocean, CDW is partially ventilated, either by direct contact with the atmosphere or by mixing with waters that have contacted the atmosphere, resulting in somewhat elevated $\Delta^{14}C$. As CDW flows northward, it ages, warms, mixes with overlying water, and slowly upwells. This upwelling, combined with mixing with overlying lower thermocline waters, results in the water mass commonly known as Pacific Deep Water (PDW). PDW has the lowest $\Delta^{14}C$ values found anywhere in the oceans. The long-term mean flow pattern for PDW is somewhat controversial; however, the radiocarbon distribution supports a southward flow with the core of the flow centered around 2500 m. WOCE results further imply that if there is a mean southward flow of PDW, it may be concentrated toward the eastward and westward boundaries rather than uniformly distributed zonally. **Figure 6** shows a zonal Pacific WOCE $\Delta^{14}C$ section at 32°S contoured at the same intervals as the previous sections. PDW is identified by the minimum layer between 2000 and 3000 m. The PDW core appears segregated into two channels, one against the South American slope and the other over the Kermadec Trench. The actual minimum values in the latter were found at ~170°W, essentially abutting the western wall of the trench. The northward-flowing CDW is also clearly indicated in this section by the relatively high $\Delta^{14}C$ values near the bottom between 140°W and the Date Line.

Little has been said about the natural $\Delta^{14}C$ values found in the upper ocean where bomb-produced radiocarbon is prevalent. GEOSECS samples were collected only ~10 years after the maximum in atmospheric $\Delta^{14}C$. GEOSECS surface water measurements almost always had the highest $\Delta^{14}C$ values. Twenty years later during WOCE, the maximum $\Delta^{14}C$ was generally below the surface.

Broecker and Peng (1982, p. 415, Figures 8–19) assembled the few surface ocean $\Delta^{14}C$ measurements

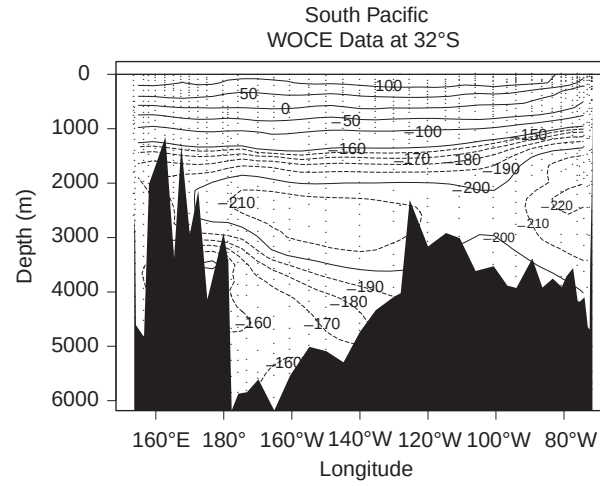

Figure 6 Zonal section of $\Delta^{14}C$ in the South Pacific collected during the WOCE program. The two minima at 2000–2500 m depth are thought to be the core of southward-flowing North Pacific Deep Water. Northward-flowing Circumpolar Deep Water is identified by the relatively high values in the Kermadec Trench area at the bottom between 140°W and the Date Line.

made prior to bomb contamination for comparison to the GEOSECS surface ocean data. For the Atlantic and Pacific Oceans, their plot of $\Delta^{14}C$ versus latitude shows a characteristic 'M' shape with maximum $\Delta^{14}C$ values of approximately -50 ppt centered in the main ocean gyres between latitudes 20° and 40°. Each ocean had a relative minimum $\Delta^{14}C$ value of approximately -70 ppt in the equatorial latitudes, 20°S to 20°N and minima at high latitudes ranging from -70 ppt for the far North Atlantic to -150 ppt for the other high latitudes. Pre-bomb measurements in the Indian Ocean are extremely sparse; however, the few data that exist imply a similar distribution. The GEOSECS surface ocean data had the same 'M' shape; however, all of the values were significantly elevated owing to bomb-derived contamination and the pattern was slightly asymmetric about the equator with the Northern Hemisphere having higher values since most of the atmospheric bomb tests were carried out there. The 'M' shape of $\Delta^{14}C$ with latitude is due to circulation patterns, the residence time of surface water in an ocean region, and air–sea gas exchange rates. At mid-latitudes the water column is relatively stable and surface waters reside sufficiently long to absorb a significant amount of ^{14}C from the atmosphere. In the equatorial zone, upwelling of deeper (and therefore lower $\Delta^{14}C$) waters lowers the surface ocean value. At high latitudes, particularly in the Southern Ocean, the near-surface water is relatively unstable, resulting in a short residence time. In these regions $\Delta^{14}C$

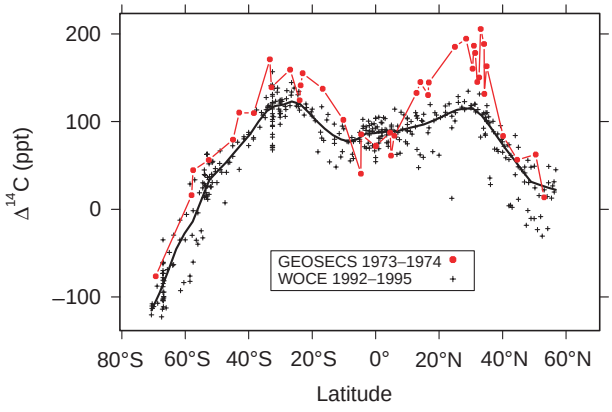

Figure 7 Distribution of $\Delta^{14}C$ in the surface Pacific Ocean as recorded by the GEOSECS program in the early 1970s and the WOCE program in the early 1990s. From **Figure 3B** it follows that GEOSECS recorded the maximum bomb-contamination. Over the 20 years separating the programs, mixing and advection dispersed the signal. By the time of WOCE the maximum contamination level was found below the surface at many locations. The asymmetry about the Equator in the GEOSECS data is a result of most atmospheric bomb tests being executed in the Northern Hemisphere.

acquired from the atmosphere is more than compensated by upwelling, mixing, and convection.

Figure 7 shows a comparison for GEOSECS and WOCE surface data from the Pacific Ocean. The GEOSECS $\Delta^{14}C$ values are higher than WOCE everywhere except for the Equator. The difference is due to two factors. First, GEOSECS sampling occurred shortly after the atmospheric maximum. At that time the air–sea $\Delta^{14}C$ gradient was large and the surface ocean $\Delta^{14}C$ values were dominated by air–sea gas exchange processes. Second, by the 1990s, atmospheric $\Delta^{14}C$ levels had declined significantly and sufficient time had occurred for ocean mixing to compete with air–sea exchange in terms of controlling the surface ocean values. During the 1990s, the maximum oceanic $\Delta^{14}C$ values were frequently below the surface. Near the Equator the situation is different. Significant upwelling occurs in this zone. During GEOSECS, waters upwelling at low latitude in the Pacific were not yet contaminated with bomb radiocarbon. Twenty years later, the upwelling waters had acquired a bomb radiocarbon component.

While surface ocean $\Delta^{14}C$ generally decreased between GEOSECS and WOCE, values throughout the upper kilometer of the water column generally increased as mixing and advection carried bomb-produced radiocarbon into the upper thermocline. The result of these processes on the bomb-produced $\Delta^{14}C$ signal can be visualized by comparing GEOSECS and WOCE depth distributions. **Figure 8** shows such a comparison. To produce this figure the WOCE data from section P16 (152°W) were gridded (center panel). GEOSECS data collected east of the data line were then gridded to the same grid (top panel). Once prepared, the two sections were simply subtracted grid box by grid box (bottom panel). One feature of **Figure 8** is the asymmetry about the Equator. The difference at the surface in **Figure 8** reflects the same information (and data) as in **Figure 7**. The greatest increase (up to 60 ppt) along the section is in the Southern Hemisphere mid-latitude thermocline at a depth of 300–800 m. This concentration change decreases in both depth and magnitude toward the Equator. All of the potential density isolines that pass through this region of significant increase (dashed lines in the bottom panel) outcrop in the Southern Ocean. These outcrops (especially during austral winter) provide the primary pathway by which radiocarbon is entering the South Pacific thermocline. In the

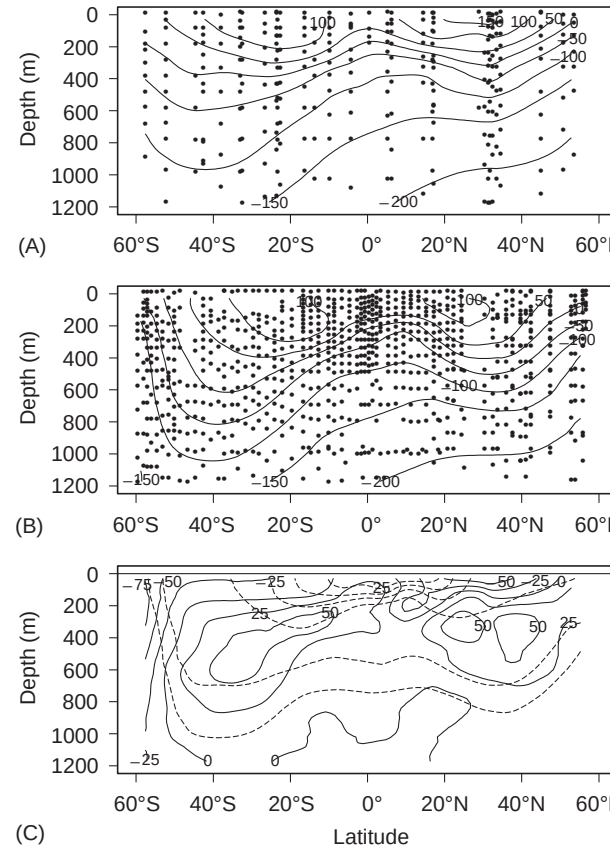

Figure 8 Panel (C) shows the change in the meridional eastern Pacific thermocline distribution of $\Delta^{14}C$ between the GEOSECS (1973–1974, (A)) and WOCE (1991–1994, (B)) surveys. The change was computed by gridding each section then finding the difference. The dashed lines in (C) indicate constant potential density surfaces. Negative near-surface values indicate maximum concentration surfaces moving down into the thermocline after GEOSECS. The region of greatest increase in the southern hemisphere is ventilated in the Southern Ocean.

North Pacific the surface ocean decrease extends as a blob well into the water column (>200 m). This large change is due to the extremely high surface concentrations measured during GEOSECS and to subsurface mixing and ventilation processes that have diluted or dispersed the peak signal. The values contoured in the bottom panel represent the change in $\Delta^{14}C$ between the two surveys, not the total bomb $\Delta^{14}C$.

WOCE results from the Indian Ocean are not yet available. Once they are, changes since GEOSECS in the South Indian Ocean should be quite similar to those in the South Pacific because the circulation and ventilation pathways are similar. Changes in the North Indian Ocean are difficult to predict owing to water inputs from the Red Sea and the Indonesian throughflow region and to the changing monsoonal circulation patterns.

Göte Östlund and Claes Rooth described radiocarbon changes in the North Atlantic Ocean using data from GEOSECS (1972) and the TTO North Atlantic Study (1981–1983). The pattern of change they noted is different from that in the Pacific because of the difference in thermohaline circulation mentioned previously. Prior to sinking, the formation waters for NADW are at the ocean surface long enough to pick up significant amounts of bomb radiocarbon from the atmosphere. The circulation pattern coupled with the timing of GEOSECS and TTO sampling resulted in increased $\Delta^{14}C$ levels during the latter program. The significant changes were mostly limited to the deep water region north of 40°N latitude. When the WOCE Atlantic samples are analyzed, we expect to see changes extending farther southward.

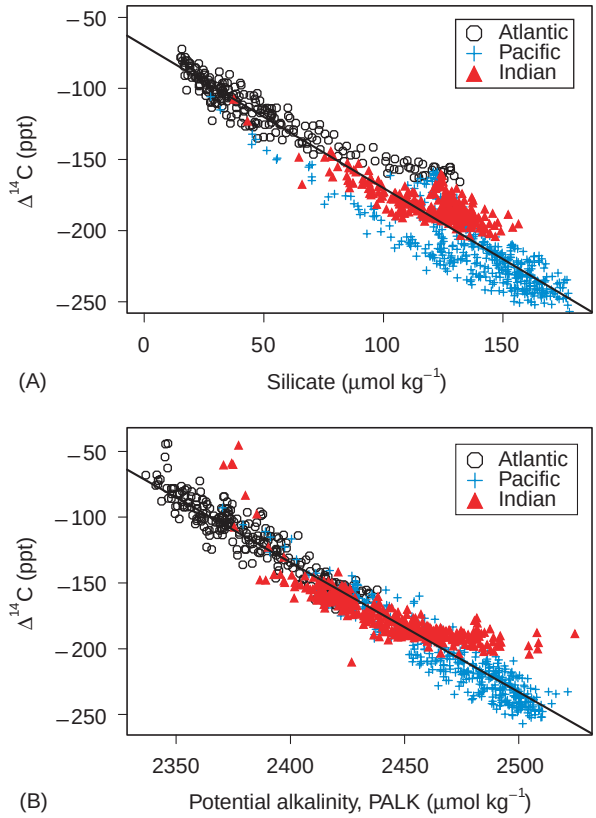

Figure 9 Comparison of the correlation of natural $\Delta^{14}C$ with silicate (A) and potential alkalinity (PALK = [alkalinity + nitrate] × 35/salinity) (B) using the GEOSECS global data. Samples from high southern latitudes are excluded from the silicate relation. The presence of tritium was used to surmise the presence of bomb-$\Delta^{14}C$. The somewhat anomalous high PALK values from the Indian Ocean are from upwelling–high productivity zones and may be influenced by nitrogen fixation and/or particle flux.

Separating the Natural and Bomb Components

Up to this point the discussion has been limited to changes in radiocarbon distribution due to oceanic uptake of bomb-produced radiocarbon. Many radiocarbon applications, however, require not the change but the distribution of either bomb or natural radiocarbon. Ocean water measurements give the total of natural plus bomb-produced $\Delta^{14}C$. Since these two are chemically and physically identical, no analytical procedure can differentiate one from the other. Far too few $\Delta^{14}C$ measurements were made in the upper ocean prior to contamination by the bomb component for us to know what the upper ocean natural $\Delta^{14}C$ distribution was.

One separation approach derived by Broecker and co-workers at LDEO uses the fact that $\Delta^{14}C$ is linearly anticorrelated with silicate in waters below the depth of bomb-^{14}C penetration. By assuming the same correlation extends to shallow waters, the natural $\Delta^{14}C$ can be estimated for upper thermocline and near surface water. Pre-bomb values for the ocean surface were approximated from the few pre-bomb surface ocean measurements. The silicate method is limited to temperate and low-latitude waters since the correlation fails at high latitudes, especially for waters of high silicate concentration. More recent work by S. Rubin and R. Key indicates that potential alkalinity (alkalinity + nitrate normalized to salinity of 35) may be a better co-variable than silicate and can be used at all latitudes. **Figure 9** illustrates the silicate and PALK correlations using the GEOSECS data set. Regardless of the co-variable, the correlation is used to estimate pre-bomb $\Delta^{14}C$ in contaminated regions. The difference between the measured and estimated natural $\Delta^{14}C$ is the bomb-produced $\Delta^{14}C$.

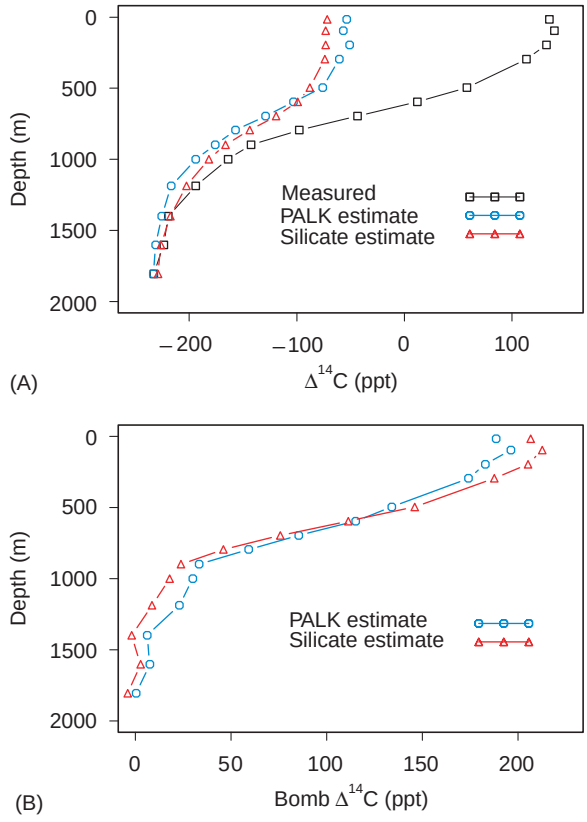

Figure 10 Panel (A) compares measured $\Delta^{14}C$ from a mid-latitude Pacific WOCE station with natural $\Delta^{14}C$ estimated using the silicate and potential alkalinity methods. Bomb-$\Delta^{14}C$, the difference between measured and natural $\Delta^{14}C$, estimated with both methods is compared in (B). Integration of estimated bomb-$\Delta^{14}C$ from the surface down to the depth where the estimate approaches zero yields an estimate of the bomb-$\Delta^{14}C$ inventory. Inventory is generally expressed in units of atoms per unit area.

In **Figure 10** the silicate and potential alkalinity (PALK) methods are illustrated and compared. The upper panel (A) shows the measured $\Delta^{14}C$ and estimates of the natural $\Delta^{14}C$ using both methods. The bomb $\Delta^{14}C$ is then just the difference between the measured value and the estimate of the natural value (B). For this example, taken from the mid-latitude Pacific, the two estimates are quite close; however this is not always true.

In **Figure 11A** the upper 1000 m of the Pacific WOCE $\Delta^{14}C$ section shown in **Figure 5C** is reproduced. **Figure 11B** shows the estimated natural $\Delta^{14}C$ using the potential alkalinity method. The shape of the two contour sets is quite similar; however, the contour values and vertical gradients are very different, illustrating the strong influence of bomb-produced radiocarbon on the upper ocean. The integrated difference between these two sections would yield an estimate of the bomb-produced $\Delta^{14}C$ inventory for the section.

Oceanographic Applications

As illustrated, the $\Delta^{14}C$ distribution can be used to infer general large-scale circulation patterns. The most valuable applications for radiocarbon derive from the fact that it is radioactive and has a half-life appropriate to the study of deep ocean processes and that the bomb component is transient and is useful as a tracer for upper ocean processes. A few of the more common uses are described below.

Deep Ocean Mixing and Ventilation Rate and Residence Time

Since the first subsurface measurements of radiocarbon, one of the primary applications has been the determination of deep ocean ventilation rates. Most of these calculations have used a box model to approximate the ocean system. The first such estimates yielded mean residence times for the various deep and abyssal ocean basins of 350–900 years. Solution of these models generally assumes a steady-state circulation, identifiable source water regions with known $\Delta^{14}C$, no mixing between water masses, and no significant biological sources or sinks. Another early approach assumed that the vertical distribution of radiocarbon in the deep and abyssal ocean could be described by a vertical advection–diffusion equation. This type of calculation leads to estimates of the effect of biological particle flux and dissolution and to the vertical upwelling and diffusion rates. The 1D vertical advection–diffusion approach has been abandoned for 2D and 3D calculations as the available data and our knowledge of oceanic processes have increased.

When the GEOSECS data became available, box models were again used to estimate residence times and mass fluxes for the abyssal ocean. In this case the model had only four boxes, one for the deep region (>1500 m) of each ocean. New bottom water formation (NADW and Antarctic Bottom Water, AABW) were included as inputs to the Atlantic and Circumpolar boxes. Upwelling was allowed in the Atlantic, Pacific, and Indian boxes and exchange was considered between the Circumpolar box and each of the other three ocean boxes. Results from this calculation gave mean replacement times of 510, 250, 275, and 85 years for the deep Pacific, Indian, Atlantic, and Southern Ocean, respectively, and 500 years for the deep waters of the entire world. Upwelling rates were estimated at 4–5 m y^{-1} and mass transports generally agreed with contemporary geostrophic calculations. Applying the same model to more recent data sets would yield the same results.

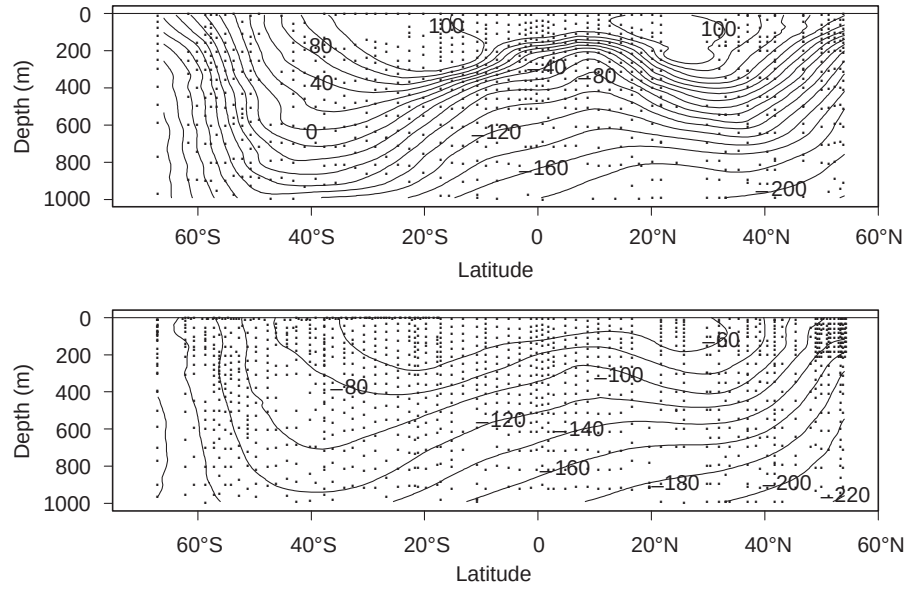

Figure 11 Upper thermocline meridional sections along 152° W in the central Pacific. (A) The same measured data as in **Figure 5C**. (B) An estimate of thermocline $\Delta^{14}C$ values prior to the invasion of bomb-produced radiocarbon.

Oxygen Utilization Rate

Radiocarbon can be used to determine the rate of biological or geochemical processes such as the rate at which oxygen is consumed in deep ocean water. The simplest example of this would be the case of a water mass moving away from a source region at a steady rate, undergoing constant biological oxygen uptake and not subject to mixing. In such a situation the oxygen utilization rate could be obtained from the slope of oxygen versus ^{14}C in appropriate units. The closest approximation to this situation is the northward transport of CDW in the abyssal Pacific, although the mixing requirement is only approximate. **Figure 12** shows such a plot for WOCE Pacific Ocean samples from deeper than 4000 m and north of 40°S. In this case, apparent oxygen utilization (saturated oxygen concentration at equilibration temperature − measured oxygen concentration) rather than oxygen concentration is plotted, to remove the effect of temperature on oxygen solubility. The least-squares slope of 0.83 μmol kg^{-1} per ppt converts to 0.1 μmol kg^{-1} y^{-1} for an oxygen utilization rate. Generally, mixing with other water masses must be accounted for prior to evaluating the gradient. With varied or additional approximations, very similar calculations have been used to estimate the mean formation rates of various deep water masses.

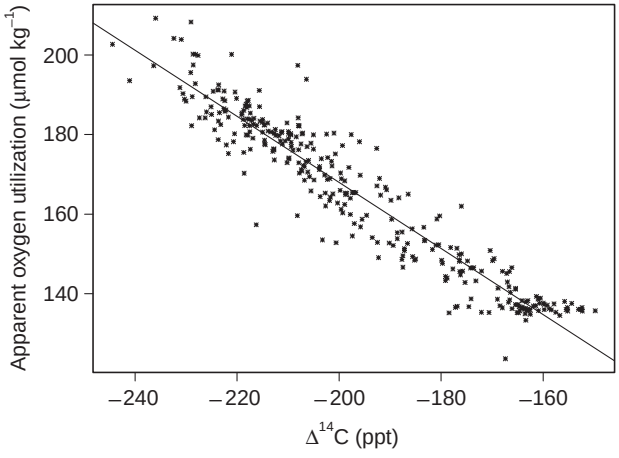

Figure 12 Apparent oxygen utilization plotted against measured $\Delta^{14}C$ for WOCE Pacific Ocean samples taken at depths greater than 4000 m and north of 40° S. The slope of the line (-0.831 ± 0.015) can be used to estimate an approximate oxygen utilization rate of 0.1 μmol kg^{-1} y^{-1} if steady state and no mixing with other water masses is assumed.

Ocean General Circulation Model Calibration

Oceanographic data are seldom of value for prediction. Additionally, the effect of a changing oceanographic parameter on another parameter can be difficult to discern directly from data. These research questions are better investigated with numerical ocean models. Before an ocean model result can be taken seriously, however, the model must demonstrate reasonable ability to simulate current conditions. This generally requires that various model inputs or variables be 'tuned' or calibrated to match measured distributions and rates. Radiocarbon is the only common measurement that can be used to

calibrate the various rates of abyssal processes in general circulation models. M. Fiadeiro carried out the first numerical simulation for the abyssal Pacific and used the GEOSECS ^{14}C data to calibrate the model. J.R. Toggweiler extended this study using a global model.

Both the Fiadeiro and Toggweiler models, and all subsequent models that include the deep water $\Delta^{14}C$, are of coarse resolution owing to current computer limitations. As the much larger WOCE ^{14}C data set becomes available, the failure of these models, especially in detail, becomes more evident. Toggweiler's model, for example, has advective mixing in the Southern Ocean that is significantly greater than supported by data. Additionally, the coarse resolution of the model prevents the formation of, or at least retards the importance of, deep western boundary currents. Significant model deficiencies appear when the bomb-^{14}C distribution and integrals at the time of GEOSECS and WOCE are compared with data.

During the last 10 years the number and variety of numerical ocean models has expanded greatly, in large part because of the availability and speed of modern computers. The Ocean Carbon Model Intercomparison Project (OCMIP) brought ocean modelers together with data experts in the first organized effort to compare model results with data, with the long-term goals of understanding the processes that cause model differences and of improving the prediction capabilities of the models. The unique aspect of this study was that each participating group essentially 'froze' development of the underlying physics in their model and then used the same boundary conditions and forcing in order to eliminate as many potential variables as possible. Radiocarbon, both bomb-derived and natural, were used as tracers in each model to examine air–sea gas exchange and long-term circulation. **Figure 13** compares results from 12 global ocean circulation models with WOCE data from section P16. The tag in the top left corner of each panel identifies the institution of the modeling group. All of the model results and the data are colored and scaled identically and the portion of the section containing bomb radiocarbon has been masked. While all of the models get the general shape of the contours, the concentrations vary widely. Detailed comparison is currently under way, but cursory examination points out significant discrepancies in all model results and remarkable model-to-model differences. Similar comparisons can be made focusing on the bomb component. Discussion of model differences is beyond the scope of this work. For information, see publications by the various groups having results in **Figure 13** (listed in **Table 1**). These radiocarbon results are not yet published, but an overview of the OCMIP-2 program can be found in the work of Dutay on chlorofluorocarbon in the same models (see Further Reading).

Air–Sea Gas Exchange and Thermocline Ventilation Rate

Radiocarbon has been used to estimate air–sea gas exchange rates for almost as long as it has been measured in the atmosphere and ocean. Generally, these calculations are based on box models, which have both included and excluded the influence of bomb contamination. W. Broecker and T.-H. Peng summarized efforts to estimate air–sea transfer rates up to 1974 and gave examples based on GEOSECS results using both natural and bomb-^{14}C and a stagnant film model. In this, the rate-limiting step for transfer is assumed to be molecular diffusion of the gas across a thin layer separating the mixed layer of the ocean from the atmosphere. In this model, if one assumes steady state for the ^{14}C and ^{12}C distribution and uniform $^{14}C/^{12}C$ for the atmosphere and surface ocean then the amount of ^{14}C entering the ocean must be balanced by decay. For this model the solution is given by eqn [3].

$$\frac{D}{z} = \frac{\sum [CO_2]|_{ocean}}{\sum [CO_2]|_{mix}} \frac{V}{A} \frac{\left[\frac{^{14}C/C|_{ocean}}{^{14}C/C|_{atm}}\right]^{\frac{\alpha_{^{14}CO_2}}{\alpha_{CO_2}}}}{1 - \left[\frac{^{14}C/C|_{mix}}{^{14}C/C|_{atm}}\right]^{\frac{\alpha_{^{14}CO_2}}{\alpha_{CO_2}}}} \lambda \quad [3]$$

Here D is the molecular diffusivity of CO_2, z is the film thickness, α_i is the solubility of i, V and A are the volume and surface area of the ocean, and λ is the ^{14}C decay coefficient. Use of pre-industrial mean concentrations gave a global boundary layer thickness of 30 μm ($D/z \sim 1800\,m\,y^{-1}$ = piston velocity). The film thickness is then used to estimate gas residence times either in the atmosphere or in the mixed layer of the ocean. For CO_2 special consideration must be made for the chemical speciation in the ocean, and for $^{14}CO_2$ further modification is necessary for isotopic effects. The equilibration times for CO_2 with respect to gas exchange, chemistry, and

Figure 13 (Right) Global ocean circulation model results from 12 different coarse-resolution models participating in OCMIP-2 compared to WOCE data for natural $\Delta^{14}C$ on a meridional Pacific section. The model groups are identified in each subpanel and in **Table 1**. All of the models used the same chemistry and boundary conditions.

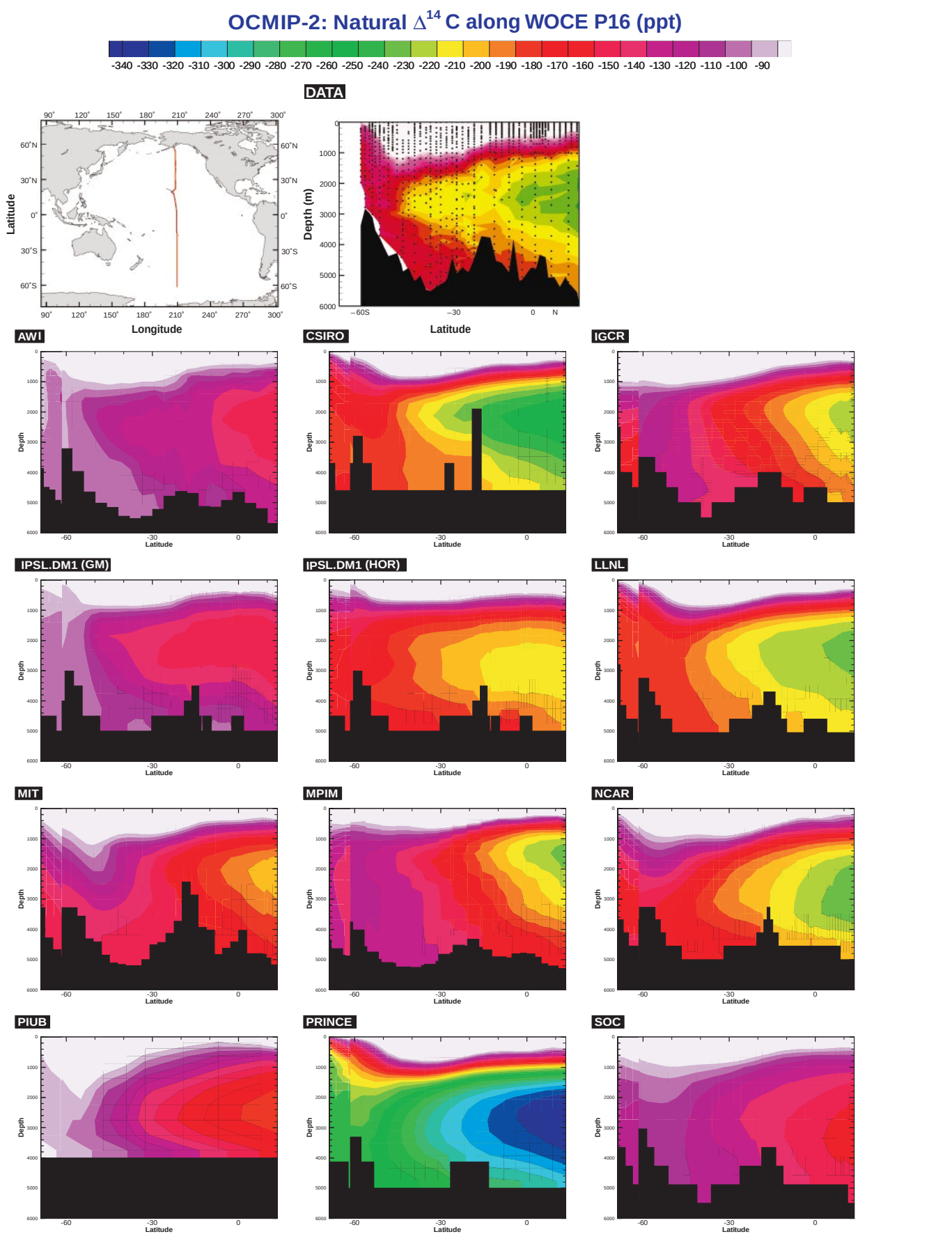
OCMIP-2: Natural Δ14 C along WOCE P16 (ppt)
-340 -330 -320 -310 -300 -290 -280 -270 -260 -250 -240 -230 -220 -210 -200 -190 -180 -170 -160 -150 -140 -130 -120 -110 -100 -90
DATA
Latitude
Longitude
Depth (m)
Latitude
AWI
CSIRO
IGCR
IPSL.DM1 (GM)
IPSL.DM1 (HOR)
LLNL
MIT
MPIM
NCAR
PIUB
PRINCE
SOC
Depth
Latitude

Table 1 OCMIP-2 participants

	Model groups
AWI	Alfred Wegener Institute for Polar and Marine Research, Bremerhaven, Germany
CSIRO	Commonwealth Science and Industrial Research Organization, Hobart, Australia
IGCR/CCSR	Institute for Global Change Research, Tokyo, Japan
IPSL	Institut Pierre Simon Laplace, Paris, France
LLNL	Lawrence Livermore National Laboratory, Livermore, CA, USA
MIT	Massachusetts Institute of Technology, Cambridge, MA, USA
MPIM	Max Planck Institut fur Meteorologie, Hamburg, Germany
NCAR	National Center for Atmospheric Research, Boulder, CO, USA
PIUB	Physics Institute, University of Bern, Switzerland
PRINCEton	Princeton University AOS, OTL/GFDL, Princeton, NJ, USA
SOC	Southampton Oceanography Centre/SUDO/Hadley Center, UK Met. Office
	Data groups
PMEL	Pacific Marine Environmental Laboratory, NOAA, Seattle, WA, USA
PSU	Pennsylvania State University, PA, USA
PRINCEton	Princeton University AOS, OTL/GFDL, Princeton, NJ, USA

isotopics are approximately 1 month, 1 year, and 10 years, respectively.

Radiocarbon has been used to study thermocline ventilation using tools ranging from simple 3-box models to full 3D ocean circulation models. Many of the 1D and 2D models are based on work by W. Jenkins using tritium in the North Atlantic. In a recent example, R. Sonnerup and co-workers at the University of Washington used chlorofluorocarbon data to calibrate a 1D (meridional) along-isopycnal advection–diffusion model in the North Pacific with WOCE data. Equation [4] is the basic equation for the model.

$$\frac{dC}{dt} = -v\frac{dC}{dx} + K\frac{d^2C}{dx^2} \qquad [4]$$

In eqn [4] C is concentration, K is along-isopycnal eddy diffusivity, $-v$ is the southward component of along isopycnal velocity, t is time, and x is the meridional distance. Upper-level isopycnal surfaces outcrop at the surface. Once the model is calibrated, the resulting values are used to investigate the distribution of other parameters. The original work and the references cited there should be read for details, but **Figure 14** shows an objective map of the bomb-^{14}C distribution on the potential density surface

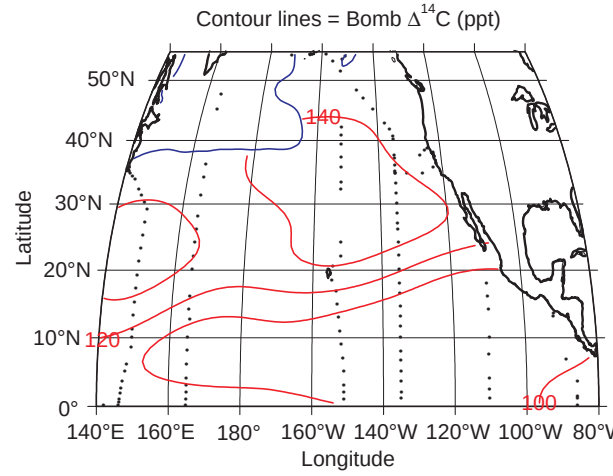

Figure 14 Bomb-Δ^{14}C on the potential density surface $\sigma_\theta = 26.1$ in the North Pacific. The blue line is the wintertime outcrop of the surface based on long-term climatology. The Sea of Okhotsk is a known region of thermocline ventilation for the North Pacific.

26.1 for the North Pacific and **Figure 15** summarizes the bomb-^{14}C distribution as a function of latitude. These figures illustrate the type of data that would be input considerations to an investigation of thermocline ventilation.

Conclusions

Since the very earliest measurements, radiocarbon has proven to be an extremely powerful tracer, and sometimes the only available tracer, for the study of many oceanographic processes. Perhaps the most important of these today are large-scale deep ocean mixing and ventilation processes and the calibration of numerical ocean models. The first global survey of the radiocarbon distribution collected on the GEOSECS program resulted in radical changes in

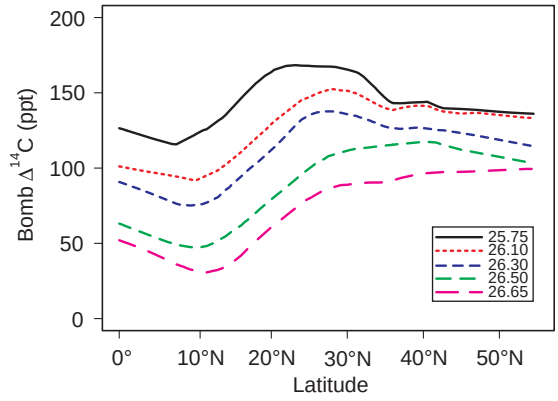

Figure 15 Meridional distribution of bomb-Δ^{14}C on potential density surfaces in the North Pacific thermocline.

the way the abyssal ocean is viewed. The newer and much denser WOCE survey will certainly add significant detail and precision to what is known and will probably result in other, if not so many, totally new discoveries. Progress with this tracer today is due largely to the decrease in required sample size from ~ 250 liters to ~ 250 milliliters and to the availability and application of fast, inexpensive computers.

See also

Abyssal Currents. Air–Sea Gas Exchange. Atmospheric Input of Pollutants. Bottom Water Formation. Carbon Cycle. Carbon Dioxide (CO_2) Cycle. Elemental Distribution: Overview. Long-term Tracer Changes. Marine Silica Cycle. Ocean Carbon System, Modelling of. Ocean Subduction. Current Systems in the Indian Ocean. Radioactive Wastes. Stable Carbon Isotope Variations in the Ocean. Thermohaline Circulation. Tracers and Large Scale Models. Tritium–Helium Dating. Water Types and Water Masses.

Glossary

dpm	Disintegrations per minute: a measure of the activity of a radioactive substance frequently used rather than concentration.
$t_{1/2}$	Half-life: time required for one half of the atoms of a radioactive species to decay.
λ	Decay constant for a radioactive species $= \ln(2)/t_{1/2}$.
Mean life, λ^{-1}	Average time expected for a given radioactive atom to decay.
Abyssal	Very deep ocean, often near bottom.
Steady state	Unchanging situation over long time interval relative to the process under consideration; frequently assumed state for the deep and abyssal ocean with respect to many parameters.

Further Reading

Broecker WS, Gerard R, Ewing M and Heezen BC (1960) Natural radiocarbon in the Atlantic Ocean. *Journal of Geophysical Research* 65(a): 2903–2931.

Broecker WS and Peng T-H (1974) Gas exchange rates between air and sea. *Tellus* 26: 21–34.

Broecker WS and Peng T-H (1982) *Tracers in the Sea*. Columbia University, Palisades, NY: Lamont-Doherty Geological Observatory.

Broecker WS, Sutherland S, Smethie W, Peng T-H and Östlund G (1995) Oceanic radiocarbon: separation of natural and bomb components. *Global Biogeochemical Cycles* 9(2): 263–288.

Craig H (1969) Abyssal carbon radiocarbon in the Pacific. *Journal of Geophysical Research* 74(23): 5491–5506.

Druffel, ERM and Griffin S (1999) Variability of surface ocean radiocarbon and stable isotopes in the southwestern Pacific. *Journal of Geophysical Research* 104(C10): 23607–23614.

Dutay JC, Bullister JL, Doney SC *et al.* (2001) Evaluation of ocean model ventilation with CFC-11: comparison of 13 global ocean models. *Global Biogeochemical Cycles* (in press).

Fiadeiro ME (1982) Three-dimensional modeling of tracers in the deep Pacific Ocean, II. Radiocarbon and circulation. *Journal of Marine Research* 40: 537–550.

Key RM, Quay PD, Jones GA *et al.* (1996) WOCE AMS radiocarbon I: Pacific Ocean results (P6, P16 and P17). *Radiocarbon* 38(3): 425–518.

Libby WF (1955) *Radiocarbon Dating*, 2nd edn. Chicago: University of Chicago Press.

Östlund HG and Rooth CGH (1990) The North Atlantic tritium and radiocarbon transients 1972–1983. *Journal of Geophysical Research* 95(C11): 20147–20165.

Schlosser P, Bönisch G, Kromer B *et al.* (1995) Mid-1980s distribution of tritium, ^{3}He, ^{14}C and ^{39}Ar in the Greenland/Norwegian Seas and the Nansen Basin of the Arctic Ocean. *Progress in Oceanography* 35: 1–28.

Sonnerup RE, Quay PD and Bullister JL (1999) Thermocline ventilation and oxygen utilization rates in the subtropical North Pacific based on CFC distributions during WOCE. *Deep-Sea Research I* 46: 777–805.

Stuiver M and Polach HA (1977) Discussion: Reporting of ^{14}C data. *Radiocarbon* 19(3): 355–363.

Stuiver M and Quay P (1983) Abyssal water carbon-14 distribution and the age of the World Ocean. *Science* 219: 849–851.

Taylor RE, Long A and Kra RS (eds) (1992) *Radiocarbon After Four Decades, An Interdisciplinary Perspective*. New York: Springer.

Toggweiler JR, Dixon K and Bryan K (1989) Simulations of radiocarbon in a coarse-resolution World Ocean model. 1. Steady state prebomb distributions. *Journal of Geophysical Research* 94(C6): 8217–8242.